Near-Infrared Spectrum of the First Excited State of Au_2^+

Special Issue

Marko Förstel,*[a] Kai Pollow,[a] Taarna Studemund,[a] and Otto Dopfer*[a]

Abstract: Au_2^+ is a simple but crucial model system for understanding the diverse catalytic activity of gold. While the Au_2^+ ground state ($X^2\Sigma_g^+$) is understood reasonably well from mass spectrometry and computations, no spectroscopic information is available for its first excited state ($A^2\Sigma_u^+$). Herein, we present the vibrationally resolved electronic spectrum of this state for cold Ar-tagged Au_2^+ cations. This exceptionally low-lying and well isolated $A^2\Sigma_{(u)}^+ \leftarrow X^2\Sigma_{(g)}^+$ transition occurs in the near-infrared range. The observed band origin (5738 cm^{-1}, 1742.9 nm, 0.711 eV) and harmonic Au–Au and Au–Ar stretch frequencies (201 and 133 cm^{-1}) agree surprisingly well with those predicted by standard time-dependent density functional theory calculations. The linearly bonded Ar tag has little impact on either the geometric or electronic structure of Au_2^+, because the Au_2^+···Ar bond (~0.4 eV) is much weaker than the Au–Au bond (~2 eV). As a result of 6 s←5d excitation of an electron from the antibonding σ_u* orbital (HOMO-1) into the bonding σ_g orbital (SOMO), the Au–Au bond contracts substantially (by 0.1 Å).

The often unusual chemical properties of small gold clusters arise from several factors, including strong spin–orbit coupling, contributions of d orbitals to chemical bonding, and large relativistic effects.[1] The typical multi-reference character of their excited electronic states, which are relevant for catalytic processes,[2] provides high challenge for quantum chemical calculations, which are required to understand electronic structure and chemical reactivity at the molecular level.[1,3] High-resolution experimental spectra provide useful benchmarks for developing and testing such quantum chemical approaches.[3,4] Recent progress in instrumentation has allowed our group to record for the first time vibrationally resolved electronic spectra of small and cold Au_n^+ cluster cations, such as Au_4^+ and Au_2^+, by means of photodissociation spectroscopy.[3,5]

Concerning Au_2^+, we have so far characterized higher excited states in the 300–700 nm range, giving rise to two complex band systems near 440 and 325 nm, which both exhibit rather irregular vibronic structure due to strong coupling of multiple electronic states occurring in the same energy range.[3a] This congested vibronic structure could only be explained by sophisticated multi-reference calculations including spin–orbit coupling and relativistic corrections.[3a] Clearly, standard time-dependent density functional theory (TD-DFT) calculations completely fail to reproduce the observed spectral pattern.[3a] Due to its high binding energy ($D_0 = 2.2 \pm 0.2$ eV),[6] the lower electronic states of Au_2^+ cannot be probed by single-photon dissociation from the cold ground electronic state. The lowest excited states of Au_n^+ clusters show a strong even-odd alternation, and the open-shell n = odd clusters have predicted transitions in the near-infrared (NIR) range.[7] In this respect, Au_{10}^+ exhibits a particularly low and broad transition centered at around 0.55 eV, which extends down into the vibrational domain of the ground electronic state. For Au_2^+, calculations predict an optically active and well isolated $A^2\Sigma_u^+$ state around 0.8 eV above the $X^2\Sigma_g^+$ ground state arising from 6 s←5d excitation of an electron from the antibonding σ_u* orbital (HOMO-1) into the bonding σ_g(s) orbital (SOMO), as shown in Figure 1.[3a,6] As no other (bright) states are nearby, coupling to other states is expected to be weak, at least near the potential minimum of the A state. As a result, the anticipated simpler vibronic spectrum may be reproduced reasonably well by standard TD-DFT calculations. The only nearby state is derived from a spin-orbit split $^2\Pi_g$ state that is optically dark (g←g transitions are parity forbidden). Another interesting feature of the A state is an avoided crossing along the Au–Au coordinate with the higher-lying $G^2\Sigma_u^+$ state of the same symmetry, leading to a potential maximum of the A state near 4 Å. To spectroscopically characterize the lowest-energy A state of Au_2^+, we add a weakly bonded inert argon atom as a tag. The Ar tag causes only a small perturbation of bare Au_2^+, because the weak van der Waals type Au_2^+···Ar bond (< 0.5 eV)[8]6ek; is substantially weaker than the chemical Au–Au bond (~2 eV).[6] Thus, in addition to reducing the temperature of Au_2^+, the Ar tag drastically reduces the effective dissociation energy of the considered cation, thereby enabling single-photon dissociation from the vibronic ground state.[7–9]

The NIR electronic spectrum of cold and mass-selected Au_2^+Ar ions shown in Figure 2 is obtained in a QP-ReTOF (quadrupole–reflectron time-of-flight) tandem mass spectrometer coupled to a temperature-controlled pulsed laser desorption source and a broadly tunable optical parametric oscillator (OPO) laser with a bandwidth of ~5 cm^{-1}.[3b,5] In short, Au_2^+Ar

[a] Dr. M. Förstel, K. Pollow, T. Studemund, Prof. Dr. O. Dopfer
Institut für Optik und Atomare Physik
Technische Universität Berlin
Hardenbergstr. 36, 10623Berlin (Germany)
E-mail: markof@physik.tu-berlin.de
dopfer@physik.tu-berlin.de

Supporting information for this article is available on the WWW under https://doi.org/10.1002/chem.202102542

Special Issue This manuscript is part of a Special Issue "Cooperative effects in heterometallic complexes".

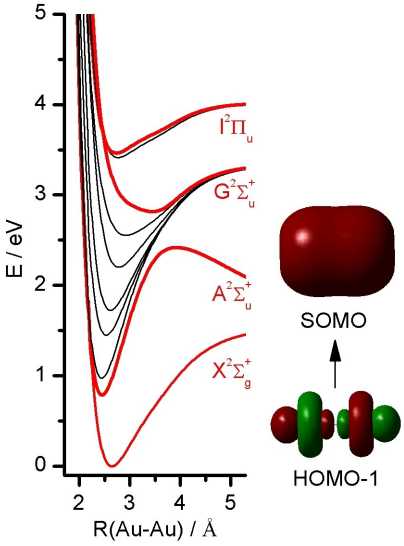

Figure 1. Potential energy curves of the doublet electronic states of Au_2^+ calculated at the unrestricted CAM-B3LYP/def2-QZVPP level. Optically allowed excited states are indicated in red. The avoided crossing between the G and A states of $^2\Sigma_u^+$ symmetry leads to a substantial change in the potential of both states. Without crossing, the G state would be dissociative, whereas the A state would have its dissociation limit near 3.5 eV. Also shown is the σ_u*(d) antibonding HOMO-1 from which the electron is excited into the bonding σ_g(s) SOMO upon A←X excitation.

clusters are generated by laser vaporization of a gold rod and expanding the resulting plasma using He carrier gas seeded with Ar (0.1%, 10 bar) into vacuum through a conical nozzle cooled by liquid nitrogen (T = 120 K). After mass selection in the QP located behind the skimmer, the Au_2^+Ar ions are guided into the extraction region of the orthogonal ReTOF, where they are overlapped in space and time with the pulsed OPO laser beam. While the OPO laser operates at 10 Hz, ions are generated at a rate of 20 Hz, allowing for recording laser-off and laser-on spectra of parent and parent plus fragment ions, respectively. The resulting signals of Au_2^+Ar parent and Au_2^+ fragment ions are integrated and plotted as a function of laser wavelength to yield the resulting NIR spectrum, which is corrected for photon flux and overlap between ion and laser beams. No other fragment channel (e.g., Au^+) is observed. The derived photodissociation cross section[5] represents a lower limit for the optical absorption cross section because it does not account for absorption into long-lived excited states and radiative decay (e.g., fluorescence).

In stark contrast to the higher excited states of Au_2^+ in the visible range,[3a] the NIR spectrum of Au_2^+Ar recorded between 5000 and 8000 cm^{-1} (Figure 2) shows a regular vibronic pattern of a single excited state of a linear molecule. No other transition is observed within 5000–10 000 cm^{-1}. Isolated vibronic peaks have a width of 5 cm^{-1}, which corresponds to the laser bandwidth and provides a lower limit for the lifetime of τ = 1 ps for the Ã state. The band origin (0^0) of the $\tilde{A}^2\Sigma^+ \leftarrow \tilde{X}^2\Sigma^+$ transition (correlating with $A^2\Sigma_u^+ \leftarrow X^2\Sigma_g^+$ for bare Au_2^+) is observed at 5738 cm^{-1} (1743 nm, 0.711 eV). A long progression of up to ten quanta in the ν_3 mode with a harmonic frequency of ω_3 = 201(1) cm^{-1} (ν_3 = 199 cm^{-1}) is assigned to the Au–Au stretch vibration, based on comparison with the higher excited states of Au_2^+ and the frequency of neutral Au_2 (ν_3 = 190 cm^{-1} in the A state).[3a,4] The long ν_3 progression peaking at n = 3 indicates a substantial change in the Au–Au bond length upon electronic excitation. Each member of the ν_3 progression is combined with a shorter progression (up to four quanta) in the ν_1 mode with ω_1 = 133(1) cm^{-1} (ν_1 = 128 cm^{-1}), which is attributed to the intermolecular Au–Ar stretch vibration. The Franck-Condon (FC) intensities of the shorter ν_1 progression suggest that the intermolecular Au_2^+···Ar interaction is only moderately affected by electronic excitation. In combination with the band origin and the low-frequency members of the $\nu_{1/3}$ progressions and combination bands, we resolve pronounced satellite peaks with a spacing of 12 cm^{-1} and decreasing intensity (inset in Figure 2). These bands are assigned to sequence hot bands (2_n^n) in the low-frequency degenerate Au–Au–Ar bending mode (ν_2), indicating that ν_2 increases by 12 cm^{-1} upon Ã←$\tilde{X}$ excitation. In contrast to $\nu_{1/3}$, there are no obvious intense progressions in ν_2, consistent with a linear structure in both electronic states. Actually, the FC analysis described below suggests the observa-

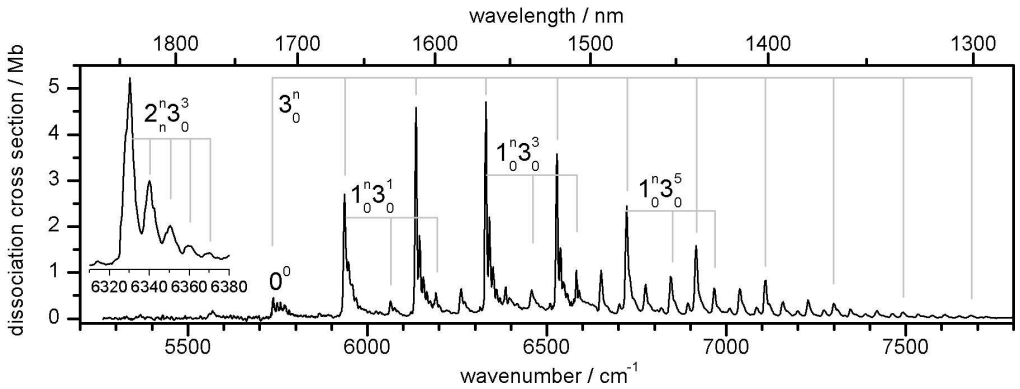

Figure 2. NIR photodissociation spectrum of the $\tilde{A}^2\Sigma^+ \leftarrow \tilde{X}^2\Sigma^+$ transition of Au_2^+Ar recorded in the Au_2^+ fragment channel at a nozzle temperature of 120 K. The two main progressions in the Au–Au and Au–Ar stretch modes (ν_3, ν_1) are indicated. The inset shows the $2_n^n3_0^3$ progression. All peak positions and assignments are listed in Table S1.

tion of weak combination bands involving two quanta in ν_2 (e.g., $2_0^2 3_0^4$ and $2_0^2 3_0^5$), resulting in $\nu_2 = 43(2)\ cm^{-1}$. From the 2_n^n sequence hot bands, we then derive the frequency of ν_2 in the $\tilde{X}$ state as $31(2)\ cm^{-1}$. The transition at $5570\ cm^{-1}$ occurs $169(3)\ cm^{-1}$ below the band origin. It does not fit into the regular pattern of $\nu_{1/3}$ and thus is assigned to the hot band in ν_3 (3_1^0). Hence, the ν_3 frequency increases from 169 to $199\ cm^{-1}$ upon $\tilde{A}\leftarrow\tilde{X}$ excitation, indicating a much stronger and shorter Au–Au bond in the A state. The harmonic frequencies and (cross) anharmonicities are obtained by fitting all vibronic transitions to a standard Dunham expansion (Table S1 in the Supporting Information), yielding harmonic frequencies of $\omega_1 = 133.08(2)\ cm^{-1}$, $\omega_3 = 200.97(2)\ cm^{-1}$, $\omega_1 x_1 = -1.33(1)\ cm^{-1}$, $\omega_3 x_3 = -0.56(1)\ cm^{-1}$, and $x_{13} = -1.33(1)\ cm^{-1}$ for the $\tilde{A}$ state. As expected, the softer Au–Ar stretch mode has a larger anharmonicity than the stiffer Au–Au stretch mode. The small number of observed quanta in ν_2 does not allow for a Dunham fit. A list with all experimental and fitted frequencies, along with vibrational assignments, is available in Table S1. All observed transitions can be reproduced to within $2.5\ cm^{-1}$ with a standard deviation of $1.0\ cm^{-1}$, which is well below the bandwidth of the employed OPO laser ($5\ cm^{-1}$).

The Birge-Sponer (BS) plot for the long progression in ν_3 (Figure 3c) yields an effective dissociation energy of $D_0 =$ 2.2(2) eV for the Au–Au bond in the A state, which would converge to the G state asymptote without avoided crossing (Figure 1). However, this BS approach does not account for the avoided crossing of the A excited state potential and thus provides only a safe upper limit for D_0. At first glance, this result is somewhat inconsistent with the reported experimental value of $D_0 = 2.2(2)$ eV for the X state obtained from mass spectrometry,[6] because the excited A state is certainly substantially more strongly bound than the ground state, as inferred from the increase in bond order and ω_3 and the contraction of the Au–Au bond upon A←X excitation (Figure 1, Table 1). Hence, the BS analysis may suggest that the D_0 value determined by mass spectrometry for the X state[6] is slightly higher than the true value, as also indicated by high-level CCSD(T) calculations ($D_0 = 1.98$ eV).[3a] However, the BS analysis suffers from several approximations. While Ar tagging has only a minor impact on the Au_2^+ potentials for the considered electronic X and A states (Table 1), the ν_3 mode is not a pure Au–Au stretch local mode, because of coupling to the Au–Ar stretch, and thus corresponds only approximately to the force constant of the Au–Au bond. Finally, the BS model is based on a Morse potential (and we probe only the lowest energy part of this potential), while the true $Au^+\cdots Au$ interaction at long range

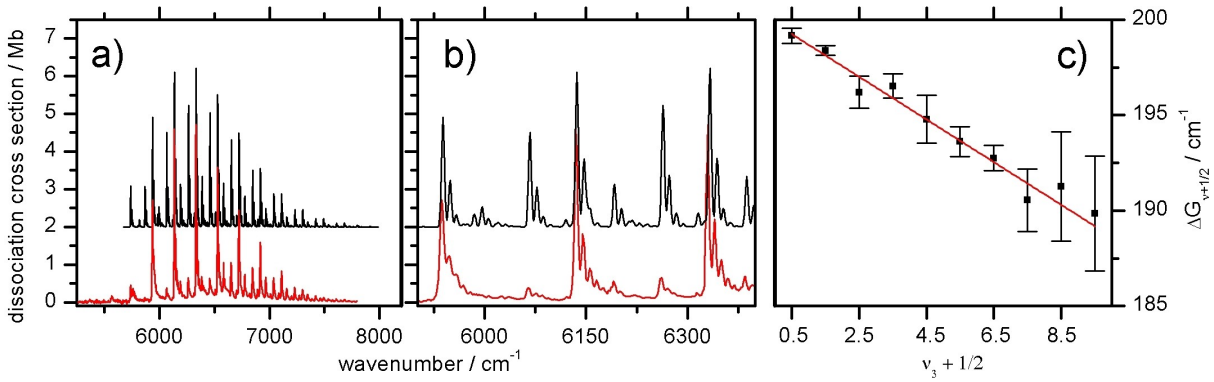

Figure 3. a) Photodissociation cross section of Au_2^+Ar into Au_2^+ and Ar (red) compared to FC simulations (black). Assignments are given in Figure 2. b) Expanded view of the spectra in (a). c) BS plot for the ν_3 progression in the $\tilde{A}^2\Sigma^+$ state of Au_2^+Ar.

Table 1. Experimental properties of the ground and first excited state of Au_2^+ and Au_2^+Ar compared to computed values.

	Experiment				CAM-B3LYP/cc-pVTZ[a]				CCSD(T)[b]	CASSCF + MRCI + SO[b]	
State	Au_2Ar^+ $\tilde{X}^2\Sigma^+$	$\tilde{A}^2\Sigma^+$	Au_2^+ $X^2\Sigma_g^+$	$A^2\Sigma_u^+$	Au_2Ar^+ $\tilde{X}^2\Sigma^+$	$\tilde{A}^2\Sigma^+$	Au_2^+ $X^2\Sigma_g^+$	$A^2\Sigma_u^+$	Au_2^+ $X^2\Sigma_g^+$	Au_2^+ $X^2\Sigma^+$	$A^2\Sigma_u^+$
E_a/eV		0.711(1)				0.79		0.77			0.95
E_v/eV		0.79(3)				0.95		0.94			1.1
R_e(Au–Ar)/Å	$\Delta(R'R'') = 0.175$[c]				2.5784	2.6927					
r_e(Au–Au)/Å	$\Delta(r'r'') = 0.09$ [c]				2.6226	2.4548	2.6345	2.4471	2.62	2.64	
$D_0(Au_2^+–Ar)$/eV	< 0.7				0.37	−0.42[d]					
D_0(Au–Au^+)/eV		< 2.2(2)	2.2(2)[e]		1.94 [f]		2.10	1.33	1.98	1.84	
ω_1/cm^{-1}		133(1)			117	131	140[g]	193[g]			
ω_2/cm^{-1}	31(2)[h]	43(2)[h]			31	41					
ω_3/cm^{-1}	169(2)[h]	201(1)			167	203					

[a] With ECP60MDF and GD3BJ. [b] Ref. [3a]. [c] Estimated from fitting computed to experimental relative intensities by variation of the difference in bond distances in FC simulations. [d] The potential of the A state converges asymptotically to that of the X state. The barrier between the minimum and local maximum of the A state potential of Au_2^+ at about $R_e = 3.8$ Å is 1.2 eV (Figure 1).[3a] [e] Ref. [6]. [f] Calculated as $E_0(AuAr^+) + E_0(Au) - E_0(Au_2^+Ar)$. [g] ω_1 in Au_2^+ corresponds to ω_3 in Au_2Ar^+ (Au–Au stretch). [h] Frequencies of fundamentals ($\nu_{2/3}$).

is dominated by charge-induced dipole interaction (depending on R^{-4}).

To confirm the assignment of the NIR spectrum, the ground and excited states of Au_2^+ and Au_2^+Ar are characterized by dispersion-corrected (TD-)DFT calculations at the unrestricted CAM-B3LYP/cc-pVTZ[10] level, including GD3BJ dispersion corrections[10b] and the ECP60MDF effective core potential (ECP),[11] as implemented in Gaussian16.[12] Calculations using the def2-tzvpp basis yield essentially the same results (Table S2). Optimized geometries and experimentally obtained harmonic frequencies and corrections are used to fit the FC intensities of the spectrum in PGOPHER.[13] To obtain the geometry differences in ground and excited state (Table 1), the atomic positions are shifted until the agreement with the experimental line intensities is optimal (Figure 3).[13] The resulting differences in the geometry are given in Table 1. While the relative intensities of ν_1 and ν_3 can be reproduced well, the intensities of the ν_1 combination bands ($1_0^n 3_0^m$) are overestimated in the simulation for low quanta of ν_3 (Figure 3b).

The properties computed for Au_2^+ and Au_2^+Ar are summarized in Table 1, along with other available computational and experimental data. The $X^2\Sigma_g$ ground state of Au_2^+ has an equilibrium bond length of $r_e = 2.6345$ Å and an Au–Au stretch frequency of 140 cm^{-1}. Its dissociation energy of $D_0 =$ 1.94 eV is in excellent agreement with the CCSD(T) value of 1.98 eV but somewhat lower than the experimental value of $D_0 = 2.2 \pm 0.2$ eV obtained from mass spectrometry[6] or $2.3 \pm$ 0.2 eV obtained by comparing the ionization potentials of the neutral atom and dimer and the neutral dissociation energy.[14] The corresponding $\tilde{X}^2\Sigma$ ground state of Au_2^+Ar is linear ($C_{\infty v}$) and no bent minimum is found on the potential. The intermolecular Au–Ar bond is characterized by $R_e = 2.578$ Å and $D_0 = 0.37$ eV, and the intermolecular harmonic stretch and bend frequencies are $\omega_1 = 117\ cm^{-1}$ and $\omega_2 = 31\ cm^{-1}$. The much stronger intramolecular Au–Au bond is characterized by $r_e =$ 2.6226 Å and $D_0 = 1.94$ eV, with a harmonic stretch frequency of $\omega_3 = 167\ cm^{-1}$, in excellent agreement with the measured value of $\nu_3 = 169\ cm^{-1}$ derived from the hot band in the NIR spectrum. Ar tagging has only a minor stabilizing effect on the Au–Au bond ($\Delta r_e = -11.9$ mÅ), probably arising from partial electron transfer (0.1 *e*) from Ar into the bonding SOMO of Au_2^+. Because of strong coupling between the Au–Au and Au–Ar local modes in the $\tilde{X}$(Au–Au stretch) corresponds to ω_1 in Au_2^+).

The first excited state of Au_2^+ is the optically bright A state ($^2\Sigma_u^+$) with a predicted adiabatic transition energy of $E_a =$ 0.77 eV and relatively low oscillator strength ($f = 0.009$). It arises from 6s←5d excitation of an electron out of the antibonding σ_u* orbital (HOMO-1) into the bonding σ_g orbital (SOMO). As a consequence of the increase in bond order, the calculated Au–Au bond contracts substantially by $\Delta r_e = -187$ mÅ and the Au–Au stretch frequency increases from 140 to 193 cm^{-1}. Because of the drastic change in geometry, there is a huge difference of 30% between adiabatic and vertical transition energy ($E_{a/v} = 0.94/0.77$ eV), indicating that reliable predictions for transition energies require optimization of the excited state. Most previous computations of Au_n^+ clusters rely merely on the calculation of vertical electronic excitations.[6,7,15] In our particular case, the predicted NIR transition shifts from 1320 to 1610 nm upon geometry optimization. Ar complexation increases the oscillator strength to $f = 0.0017$ and has only a minor stabilizing impact on the Au–Au bond in the Ã state ($\Delta r_e = -7.7$ mÅ, $\Delta\omega_2 = +12\ cm^{-1}$). Overall, Ã←$\tilde{X}$ excitation of Au_2^+Ar leads to a substantial contraction of the strong Au–Au bond ($\Delta r_e = -168$ mÅ) and a similar elongation of the soft Au–Ar bond ($\Delta R_e = 114$ mÅ). While the strengthening of the Au–Au bond is well reflected by the increase in ω_3 from 167 to 203 cm^{-1}, the weakened Au–Ar bond also exhibits an increase in ω_1 from 117 to 131 cm^{-1}. This at first glance inconsistent picture arises from the change in coupling between the Au–Ar and Au–Au local modes upon Ã←$\tilde{X}$ excitation. While both modes are strongly coupled in the $\tilde{X}$ state leading to an enhanced splitting between both normal modes, they become almost decoupled in the Ã state. The frequency of the degenerate intermolecular bending mode ω_2 increases from 31 to 43 cm^{-1} (or 40%), indicating a much stiffer bending potential in the Ã state, with higher angular anisotropy.

Overall, the (TD-)DFT calculations reproduce the experimental observation to high accuracy. The assigned band origin at 5738 cm^{-1} (0.711(2) eV) agrees well with the predicted value (0.79 eV). Ar complexation changes E_a and E_0 of Au_2^+ by only 0.02 and 0.01 eV, respectively, thus confirming that the Ar tag has essentially no effect on this electronic transition. The measured frequencies in the Ã state ($\omega_{1/3} = 133/201\ cm^{-1}$) agree with the computed ones (131/203 cm^{-1}) to within 2 cm^{-1}. The computed increase of 10 cm^{-1} in ω_2 upon Ã←$\tilde{X}$ excitation is close to the observed spacing of 12 cm^{-1} in the 2_n^n sequence hot band progression. Similarly, the ν_3 frequency in the $\tilde{X}$ state (169 cm^{-1}) assigned from the hot band is consistent with the predicted value of $\omega_3 = 167\ cm^{-1}$. This overall excellent quantitative match between experiment and computation with respect to electronic transition energy and all vibrational frequencies illustrates that the employed standard (TD-)DFT calculations are surprisingly well suited to reliably describe the chemical bonding and electronic structure of the X and A state of Au_2^+, and is rationalized by the, at most, small perturbation of these isolated electronic states (Figure 1). This scenario is not true anymore for the higher excited states, which are strongly coupled.[3a]

The relative intensities of the hot band transitions may be used to estimate the effective vibrational temperature of the cluster ions. Assuming thermal equilibrium (Boltzmann distribution) and similar FC factors for the hot band and fundamental of ν_3 (3_1^0 and 3_0^1), their observed intensity ratio of 1:10 reflects directly the population ratio of the ν_3 and ground states. This ratio corresponds to a temperature of around 110 K, which agrees well with the nozzle temperature of $T = 120$ K. The ion temperature can also be estimated from the population of the ν_2 levels in the $\tilde{X}$ state derived from the observed sequence hot bands spaced by 12 cm^{-1}, again assuming the same FC factors. For example, the intensity ratio of $3_0^n{:}3_0^n2_1^1{:}3_0^n2_2^2$ with $n = 1$–3 is within 4.8:1.8:1.0 and 1.5:1.2:0.9, and varies between different scans with equal source conditions but also within single scans. Again, assuming a Boltzmann distribution, these ratios translate into $T = 50$–200 K, respectively. The FC simulations show a

slightly different picture. To achieve good agreement in the hot band contributions, we need to consider a different temperature for ν_2 compared to ν_1 and ν_3. The best fit is obtained with a ν_2 temperature of around 25 K, while ν_1 and ν_3 have an effective temperature of around 200 K. This result is not surprising because low-frequency modes cool more efficiently than high-frequency vibrations.

In summary, we have characterized the previously elusive first electronically excited A state of the fundamental Au_2^+ diatomic cation by means of high-resolution photodissociation spectroscopy of the Ar-tagged ion. Significantly, the measured A←X spectrum provides the first spectroscopic information about the chemical bonding of Au_2^+ in both the ground and first excited state. The exceptionally low-lying excited A state occurring in the NIR range is dominated by a long vibrational progression in the Au–Au stretch mode caused by a substantial bond contraction upon electronic excitation. This change in geometry is caused by one-electron excitation from an antibonding σ_u* orbital into the bonding σ_g orbital. The vibronically resolved spectrum allows for the determination of all three vibrational modes in the Ã state of Au_2^+Ar and of two frequencies in the $\tilde{X}$ state via hot band analysis. Analysis of anharmonicity provides a safe upper limit of the dissociation energy in the A state as 2.2(2) eV. The true dissociation energy should be substantially lower because the BS analysis does not account for the effects of the avoided crossing of the A state with a higher lying excited state. Significantly, the TD-DFT calculations describe the properties of the largely isolated X and A state to surprisingly high accuracy (as seen for example also by the negligible spin contamination of $<2\%$), given that an excited state of such a heavy diatomic open-shell cation is considered and that the properties of higher excited states cannot be reproduced at such level of theory.[3a] Comparison between Au_2^+ and Au_2^+Ar reveals that rare gas tagging has essentially no impact on the geometric and electronic structure of the diatomic cation, while electronic excitation reduces the coupling between the Au–Au and Au–Ar stretch modes.

Recent computations predict that open-shell Au_n^+ clusters with even n ($n \leq 12$) have low-energy electronic states in the NIR range. The most extreme case in this size range is Au_{10}^+, for which the onset of a rather broad and unresolved band is observed (also by Ar tagging), with a fitted maximum near 5000 cm^{-1} (~0.6 eV, ~2000 nm) and a width of ~4400 cm^{-1} (~0.55 eV). This band has been attributed to three overlapping LUMO←SOMO electronic transitions, and its large width has been rationalized by spectral congestion from unresolved vibronic excitation, vibronic coupling of the Jahn-Teller distorted tetrahedral structure, and/or lifetime broadening.[7] In contrast to the larger and more complex Au_{10}^+ cluster, the lowest-energy NIR excitation of Au_2^+ observed at 0.71 eV arises from a single and well-isolated SOMO←HOMO-1 transition resulting in a regular well-resolved electronic spectrum, with a long-lived excited state ($\tau \geq 1$ ps). Significantly, the Au_2^+Ar spectrum allows the determination of all vibrational frequencies, thereby providing very detailed information about the Au–Au and Au–Ar bonds as a function of electronic excitation. Such highly resolved electronic spectra are still rare for transition metal clusters.[3,8a,16]

Acknowledgements

This project was supported by Deutsche Forschungsgemeinschaft (DFG, DO 729/9). We thank Roland Mitric and André Fielicke for helpful discussions. Open Access funding enabled and organized by Projekt DEAL.

Conflict of Interest

The authors declare no conflict of interest.

Keywords: cations · electronic structure · gold · photodissociation · structure elucidation

[1] a) H. Schwarz, *Angew. Chem. Int. Ed.* **2003**, *42*, 4442–4454; *Angew. Chem.* **2003**, *115*, 4580–4593; b) P. Schwerdtfeger, M. Dolg, W. E. Schwarz, G. A. Bowmaker, P. D. Boyd, *J. Chem. Phys.* **1989**, *91*, 1762–1774; c) P. Pyykkö, *Angew. Chem. Int. Ed.* **2004**, *43*, 4412–4456; *Angew. Chem.* **2004**, *116*, 4512–4557; d) P. Pyykkö, *Chem. Rev.* **1988**, *88*, 563–594; e) D. J. Gorin, F. D. Toste, *Nature* **2007**, *446*, 395–403.

[2] a) N. S. Shuman, S. G. Ard, B. C. Sweeny, A. A. Viggiano, C. J. Owen, P. B. Armentrout, *J. Phys. Chem. A* **2020**, *124*, 3335–3346; b) N. S. Shuman, S. G. Ard, B. C. Sweeny, H. Pan, A. A. Viggiano, N. R. Keyes, H. Guo, C. J. Owen, P. Armentrout, *Catal. Sci. Technol.* **2019**, *9*, 2767–2780; c) S. M. Lang, T. M. Bernhardt, V. Chernyy, J. M. Bakker, R. N. Barnett, U. Landman, *Angew. Chem. Int. Ed.* **2017**, *56*, 13406–13410; *Angew. Chem.* **2017**, *129*, 13591–13595; d) L. D. Socaciu, J. Hagen, T. M. Bernhardt, L. Wöste, U. Heiz, H. Häkkinen, U. Landman, *J. Am. Chem. Soc.* **2003**, *125*, 10437–10445; e) A. Sanchez, S. Abbet, U. Heiz, W.-D. Schneider, H. Häkkinen, R. Barnett, U. Landman, *J. Phys. Chem. A* **1999**, *103*, 9573–9578; f) A. Shayeghi, R. Schäfer, D. Rayner, R. Johnston, A. Fielicke, *J. Chem. Phys.* **2015**, *143*, 024310; g) A. Fielicke, G. von Helden, G. Meijer, D. B. Pedersen, B. Simard, D. M. Rayner, *J. Am. Chem. Soc.* **2005**, *127*, 8416–8423.

[3] a) M. Förstel, K. M. Pollow, K. Saroukh, E. A. Najib, R. Mitric, O. Dopfer, *Angew. Chem. Int. Ed.* **2020**, *59*, 21403–21408; *Angew. Chem.* **2020**, *132*, 21587–21592; b) M. Förstel, W. Schewe, O. Dopfer, *Angew. Chem. Int. Ed.* **2019**, *58*, 3356–3360; *Angew. Chem.* **2019**, *131*, 3394–3398.

[4] G. A. Bishea, M. D. Morse, *J. Chem. Phys.* **1991**, *95*, 5646–5659.

[5] M. Förstel, B. K. A. Jaeger, W. Schewe, P. H. A. Sporkhorst, O. Dopfer, *Rev. Sci. Instrum.* **2017**, *88*, 123110.

[6] C. J. Owen, N. R. Keyes, C. Xie, H. Guo, P. Armentrout, *J. Chem. Phys.* **2019**, *150*, 174305.

[7] A. E. Green, A. S. Gentelman, W. Schöllkopf, A. Fielicke, S. R. Mackenzie, *Phys. Rev. Lett.* **2021**, *127*, 033002 .

[8] a) A. Schweizer, J. M. Weber, S. Gilb, H. Schneider, D. Schooss, M. M. Kappes, *J. Chem. Phys.* **2003**, *119*, 3699–3710; b) A. Shayeghi, R. L. Johnston, D. M. Rayner, R. Schäfer, A. Fielicke, *Angew. Chem. Int. Ed.* **2015**, *54*, 10675–10680; *Angew. Chem.* **2015**, *127*, 10822–10827; c) S. M. Lang, P. Claes, N. T. Cuong, M. T. Nguyen, P. Lievens, E. Janssens, *J. Chem. Phys.* **2011**, *135*, 224305.

[9] a) M. Okumura, L. Yeh, J. Myers, Y. T. Lee, *J. Phys. Chem.* **1990**, *94*, 3416–3427; b) K. R. Asmis, J. Sauer, *Mass Spectrom. Rev.* **2007**, *26*, 542–562; c) O. Dopfer, *Z. Phys. Chem.* **2005**, *219*, 125–168; d) E. J. Bieske, O. Dopfer, *Chem. Rev.* **2000**, *100*, 3963–3998; e) A. N. Gloess, H. Schneider, J. M. Weber, M. M. Kappes, *J. Chem. Phys.* **2008**, *128*, 114312; f) B. K. A. Jaeger, M. Savoca, O. Dopfer, N. X. Truong, *Int. J. Mass Spectrom.* **2016**, *402*, 49–56; g) A. Fielicke, A. Kirilyuk, C. Ratsch, J. Behler, M. Scheffler, G. von Helden, G. Meijer, *Phys. Rev. Lett.* **2004**, *93*, 023401.

[10] a) T. Yanai, D. P. Tew, N. C. Handy, *Chem. Phys. Lett.* **2004**, *393*, 51–57; b) D. E. Woon, T. H. Dunning, Jr, *J. Chem. Phys.* **1993**, *98*, 1358–1371.

[11] D. Figgen, G. Rauhut, M. Dolg, H. Stoll, *Chem. Phys.* **2005**, *311*, 227–244.

[12] M. J. Frisch, et al., *Gaussian16*, *Rev. A03*, Gaussian, Inc., Wallingford, CT, **2016**.
[13] C. M. Western, *J. Quant. Spectrosc. Radiat. Transfer* **2017**, *186*, 221–242.
[14] a) M. Cheeseman, J. Eyler, *J. Phys. Chem.* **1992**, *96*, 1082–1087; b) S. Gilb, P. Weis, F. Furche, R. Ahlrichs, M. M. Kappes, *J. Chem. Phys.* **2002**, *116*, 4094–4101.
[15] a) A. Shayeghi, L. Pašteka, D. Götz, P. Schwerdtfeger, R. Schäfer, *Phys. Chem. Chem. Phys.* **2018**, *20*, 9108–9114; b) A. Shayeghi, C. Heard, R. Johnston, R. Schäfer, *J. Chem. Phys.* **2014**, *140*, 054312.
[16] M. F. Jarrold, K. M. Creegan, *Chem. Phys. Lett.* **1990**, *166*, 116–122.

Manuscript received: July 19, 2021
Accepted manuscript online: August 23, 2021
Version of record online: September 15, 2021

